Available online at www.sciencedirect.com

SCIENCE DIRECT®

Earth and Planetary Science Letters 230 (2005) 379–395

EPSL

www.elsevier.com/locate/epsl

The role of chemical boundary layers in regulating the thickness of continental and oceanic thermal boundary layers

Cin-Ty Aeolus Lee*, Adrian Lenardic, Catherine M. Cooper, Fenglin Niu, Alan Levander

Department of Earth Science, MS-126, Rice University, 6100 Main St., Houston, TX 77005, United States

Received 6 July 2004; received in revised form 10 November 2004; accepted 23 November 2004
Available online 13 January 2005
Editor: S. King

Abstract

An important feature of continents and oceans is that they are underlain by chemically distinct mantle, made intrinsically buoyant and highly viscous by melt depletion and accompanying dehydration, respectively. Of interest here are the influences of these preexisting chemical boundary layers on small-scale convective processes (as opposed to large-scale processes, which govern the drift of continents and the eventual fate of oceanic thermal boundary layers, e.g., subduction) at the base of the oceanic and continental thermal boundary layers. This manuscript explores the endmember in which dehydrated and melt-depleted boundary layers are assumed to be strong (in the viscous sense) and chemically buoyant enough that they do not partake in any secondary convection, that is, vertical heat transfer through these lids occurs purely by conduction. This assumption implies that the only part of the thermal boundary layer that participates in secondary convection resides beneath the strong chemical boundary layer. For oceans, this leads to the condition that the onset time of convective instability is suppressed until after the thermal boundary layer has cooled through the base of the strong chemical boundary layer, whose thickness is defined at the outset by the depth at which the solid mantle adiabat crosses the anhydrous peridotite solidus. A scaling law is presented that accounts for the presence of a preexisting strong chemical boundary layer and predicts that the onset time of convective instability beneath oceans correlates with the thickness of the chemical boundary layer, which itself correlates with the potential temperature of the mantle at the time of melting. Estimated paleo-potential temperatures required to generate old oceanic crust in the Pacific and Atlantic may in fact be correlated with onset time of seafloor flattening, but more data are needed to confirm these preliminary observations. Finally, for continents, recent numerical models suggest that the thickness of the convective sublayer, hence the total thermal boundary layer thickness, is also controlled by the thickness of a preexisting strong chemical boundary layer. Xenolith data from cratons are shown to be largely consistent with the model-predicted relationship between the thicknesses of the chemical and thermal boundary layers beneath continents. The conclusion of this study is that the nature of both oceanic and continental thermal boundary layers is likely to be linked to preexisting strong chemical boundary layers.

Keywords: craton; peridotite; chemical boundary layer; dehydration; flattening

* Corresponding author. Tel.: +1 713 348 5084; fax: +1 713 348 5214.
E-mail address: ctlee@rice.edu (C.-T.A. Lee).

0012-821X/$ - see front matter © 2004 Elsevier B.V. All rights reserved.
doi:10.1016/j.epsl.2004.11.019

1. Introduction

One of the most important observations made during the early developments of plate tectonic theory was that the depth of young seafloor (<70–100 Ma) on average increases with the square root of the crust's age and that the accompanying heat flow decreases as the inverse of the square root of age [1] (Fig. 1). It was subsequently shown that the $t^{1/2}$ relationships could be explained by approximating the growth of the upper thermal boundary layer (the boundary layer over which the mode of heat transfer changes from thermal buoyancy-driven advection to conduction) of the Earth's convecting interior by an infinite half-space conductive cooling model [1]. This model, which we refer to as the boundary layer model, predicts that the thickness of the thermal boundary layer scales monotonically with the square root of seafloor age according to the relationship, $L \sim \sqrt{4\kappa t}$, where L is the thermal thickness, t is time, and κ is thermal diffusivity. For a thermal diffusivity of ~30 km^2/Ma, this relationship takes the form, $L \sim 11\sqrt{t}$, where L is in km and t is in Ma. By accounting for thermal contraction and the decrease in thermal gradient across the growing thermal boundary layer, the evolution of seafloor depth and heat flow with time follows accordingly. The success of the boundary layer model in linking the kinematics of seafloor spreading to the depth and heat flow of young seafloor represents the strongest evidence so far that plate tectonics and mantle convection are linked [2].

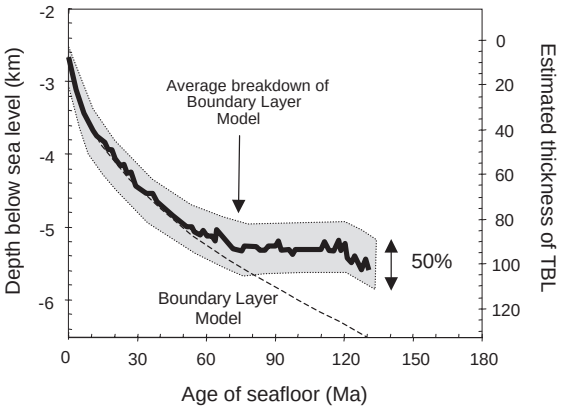

Fig. 1. Plot showing the median depth of the seafloor (black line; left-hand axis) as a function seafloor age using global compilation of seafloor bathymetry data [3]; shaded area represents the upper and lower quartiles of depth. Dashed line indicates the predicted seafloor depth assuming instantaneous boundary layer cooling of an infinite half-space. Right vertical axis represents a rough estimate of the corresponding thermal thickness beneath oceans.

Global bathymetry studies, however, show that for old seafloor (>70 Ma), heat flow and seafloor depth deviate from the boundary layer cooling model and saturate at regionally constant values (e.g., Fig. 1; [3] and references therein). Saturation of seafloor depth and heat flow further implies that the thickness of the thermal boundary layer beneath the seafloor also saturates at depths corresponding to the depth at which the boundary layer cooling model breaks down ($L \sim 11\sqrt{t_c}$, where t_c is the breakdown time). Similarly, the thicknesses of continental thermal boundary layers also appear to be thinner than predicted by conductive cooling alone. As we will discuss below, this discrepancy is most pronounced for Archean cratons (>2.5 Gy old) where the observed thickness of the thermal boundary layer is 200–300 km, but that predicted by conductive cooling is 400–500 km.

Most of the hypotheses that have been proposed to explain the eventual breakdown of the half-space conductive cooling model invoke a transition from a conductive to some sort of convective or advective system. One class of models invokes the onset of small-scale convective instabilities at the base of the thermal boundary layer [2,4,5]. An endmember in this class of models describes oceanic lithosphere as a rigid plate of constant thickness through which heat is transferred by conduction and whose base is kept at a constant temperature presumably by secondary convection processes [6,7]. However, Phipps Morgan [8] and Davies [9] pointed out that these secondary convection models fail to explain the fact that although the time at which the boundary layer cooling model breaks down occurs on average at 70 Ma, the onset time of seafloor flattening actually varies regionally, as shown by Marty and Cazenave [10]. This is further borne out by the fact that the saturation values of heat flow and seafloor depth also display regional variation [10]. This led Phipps Morgan and Davies to prefer other models to explain the observed flattening of old seafloor. For example, Phipps Morgan suggests pressure forces in the low viscosity asthenospheric channel beneath the oceanic thermal boundary layer might be responsible for the anomalous bathymetry and heat flow of old seafloor [8].

Alternatively, hotspots have been called upon to convectively thin the lithosphere [11].

Here, we explore the possibility that preexisting chemical/rheologic boundary layers beneath oceans and continents might dictate the thickness of thermal boundary layers by influencing secondary convective processes at the base of the thermal boundary layer. We are not concerned with large-scale convective processes, which govern the drift of continents and the eventual fate of oceanic thermal boundary layers, i.e., subduction. Our paper is largely motivated by recent advances in the community's understanding of the deep thermal and compositional structure of continents, particularly beneath their ancient tectonically quiescent cores (cratons). Cratons are typically underlain by thick mantle keels, which are highly depleted in meltable components [12]. Oceanic mantle has also experienced melt extraction although not to the very high extents seen in cratonic mantle. Importantly, melt depletion results in a mantle residue that is not only chemically buoyant but also dehydrated, the latter which results in an increase in intrinsic viscosity, possibly by more than two orders of magnitude [13,14]. The effects of enhanced chemical buoyancy and viscosity are to compete against the development of convective instabilities. Such chemical boundary layers may thus be expected to a play a role in the development and preservation of continental and oceanic thermal boundary layers. At least beneath continents, radiogenic isotopic studies indicate that these chemical boundary layers have remained isolated and largely undeformed over billion year timescales [15,16].

The effects of chemical buoyancy on the development and preservation of thermal boundary layers have recently been investigated by Zaranek and Parmentier [17] and Sleep [18], respectively. Although the effects of temperature-dependent viscosity have already been investigated (e.g., [19,20]), the influence of depth-dependent viscosity, specifically, intrinsic depth-variations in viscosity, have only recently been investigated by Korenaga and Jordan [4]. The purpose of our paper is to assess the endmember in which the chemical boundary layer, as a consequence of dehydration and chemical buoyancy, can be considered a purely (vertically) conductive lid such that it effectively does not participate in secondary convection. We consider how a preexisting and rheologically strong chemical boundary layer influences the thickness of thermal boundary layers beneath continents and oceans. We begin with a review of the main properties of cratonic mantle that are likely to influence its long-term stability and strength: density, water content, and thermal state. We then show that saturation thicknesses of thermal boundary layers predicted by the recent numerical models of Cooper et al. [21] are broadly consistent with xenolith data. In the case of oceans, we present a scaling analysis that provides qualitative predictions on the relationship between the onset time of convective instabilities and the thickness of the chemical boundary layer.

2. The cratonic perspective: long-lived chemical boundary layers

We begin by reviewing the most relevant characteristics of cratonic mantle. A distinct feature of cratonic mantle keels is that their major-element composition, as inferred from mantle xenoliths, differs from that of the shallow part of the convecting mantle from which mid-ocean ridge basalts derive [12,22,23]. Compared to convecting mantle, mantle keels are highly depleted in Ca and Al and to a lesser extent Fe. Ca and Al are the elements that stabilize clinopyroxene and garnet, both of which are the first minerals to be exhausted during progressive partial melt extraction. The depletion in Ca and Al is believed to be the result of extensive melt extraction (20–40 wt.% partial melt). A common index of melt extraction is the Mg# (the molar ratio Mg/(Mg+Fe)), which is a measure of the relative proportion of Fe to Mg. Convecting mantle is more "fertile" in terms of meltable components and is characterized by Mg#s of ~0.88–0.89. Cratonic mantle keels are largely depleted of meltable components (clinopyroxene and garnet) and are characterized by average Mg#s of ~0.92–0.93. Fertile (low Mg#) peridotites found in cratonic xenolith suites appear to originate from a distinct narrow zone below the chemically depleted layer.

There are two important consequences of high degrees of melt extraction. The first is that the residue becomes intrinsically less dense because the dense minerals, garnet and clinopyroxene, are exhausted and the proportion of Fe relative to Mg

decreases (e.g., Mg# increases) [12,22,24,25]. Jordan suggested that this decrease in intrinsic density may offset the increase in density of mantle keels due to thermal contraction associated with the cooler thermal state of cratons relative to the convecting mantle [26]. Using the South African craton as an example, he proposed that mantle keels are in fact neutrally buoyant because the compositional buoyancy exactly offsets the negative thermal buoyancy of cratons at every depth, a condition that Jordan termed "isopycnic." The large amount of data since accumulated for other cratonic mantle keels [23,27–29] has confirmed that high Mg# peridotite indeed characterizes the bulk of cratonic mantle. Although it now appears that cratonic mantle may not be strictly isopycnic at every depth (see Fig. 2), the depth-integrated density of cratonic mantle indeed roughly offsets the craton's total negative thermal buoyancy.

The second consequence of melt extraction is the progressive dehydration of the solid residue due to the incompatible nature of H_2O during partial melting [14]. At the high degrees of melting required to generate the high Mg#s of cratonic mantle peridotites (>30% melting), the residual peridotites should have been completely dehydrated. Estimates of the amount of H_2O in different parts of the mantle range from ~100 to 750 ppm ([30–32] and references therein). According to Hirth and Kolhstedt [14], such dehydration can lead to a 500-fold increase in intrinsic viscosity. Assuming subsequent metasomatism did not pervasively reintroduce water to the dehydrated mantle keel, the chemically depleted boundary layer then represents a layer of low intrinsic density and increased intrinsic viscosity (c.f., [13,33]).

The precise thickness of the chemical boundary layer (δ_{CBL}) and/or thermal boundary layer (δ_{TBL}) beneath cratons is debated. Seismic tomographic studies show

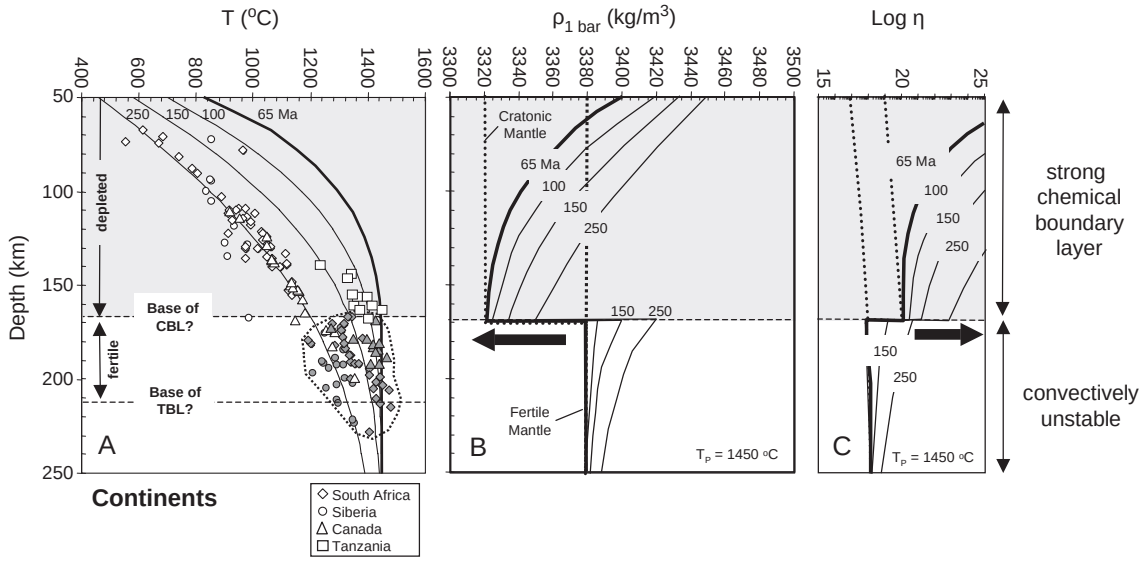

Fig. 2. (A) Thermal state of Archean cratonic mantle based on xenolith thermobarometric data from various cratons [28,29,40]. Xenoliths from shallower than ~175 km are mostly highly depleted (open symbols; chemical boundary layer; chemical boundary layer), whereas those deeper than ~175 km are mostly fertile (gray symbols). Curved lines represent hypothetical transient boundary layer cooling geotherms at different times. (B) Pressure-normalized density structure of cratonic mantle as a function of different thermal states defined by the transient geotherms shown in panel (A). Dotted lines represent the density of cratonic and fertile mantle at 25 °C. C. Log viscosity (η; Pa s) as a function of depth for different transient geotherms. Viscosities are calculated following Hirth and Kohlstedt [14] for non-Newtonian fluids using $\eta = A^{-1}\,\sigma^{n-1}\exp((E+PV)/(RT))$ where P is pressure (Pa), T is temperature (K), A is the preexponential factor ($s^{-1}MPa^{-n}$), E is the activation energy (kJ/mol), V is the activation volume (m^3/mol), n is the exponent (assumed to be 3.5) and σ is the background deviatoric stress (~0.3 MPa); olivine rheology was assumed (dry: $A=4.85\times10^4$, $E=535$; wet: $A=4.89\times10^6$, $E=515$). The activation volume V was assumed to change linearly from 15×10^{-6} at 1 bar to 7.5×10^{-6} at 8 GPa following [14]. Solid curves represent viscosities for the transient geotherms in panel (A). Dotted lines represent the viscosities for cratonic and fertile mantle at T_P.

that the high velocities beneath cratons extend to depths anywhere from 200 to 400 km [34–37]. This large uncertainty may be due to the lack of good vertical resolution in the teleseismic data used in tomographic studies [38,39]. In addition, seismic velocities are most sensitive to temperature, and therefore, high-velocity anomalies at great depth may simply reflect local thermal disturbances rather than the presence of a thick chemical boundary.

Xenolith thermobarometric data provide an independent constraint on the thickness of the chemical and thermal boundary layers provided the xenoliths were in chemical equilibrium up until the time they were sampled by their host volcanics. The thermobarometric data of xenoliths indicate that chemically depleted mantle extends to depths of ~175 km [23,29,40,41] (open symbols in Fig. 2A). Beyond this depth, there appears to be a pronounced increase in the fertility of mantle xenoliths (gray symbols in Fig. 2A). The equilibration temperatures of these deep and fertile xenoliths range between 1300 and 1450 °C, approaching the temperature defined by the solid mantle adiabat at equivalent depths. Several interpretations for the origin of these deep, fertile xenoliths have been suggested: high Mg# peridotites that have been reenriched (refertilized) in Fe, Ca, and Al (some show disequilibria in the form of chemically zoned minerals and high strain deformation textures) [15,42], subducted oceanic lithospheric mantle [43], and/or samples from the top of the fertile convecting mantle [42]. Whatever their origin, the deep, fertile xenoliths appear to derive from just below the chemically depleted layer. If we interpret them to derive from the lower part of the thermal boundary layer, their near-adiabatic temperatures suggest that the base of the thermal boundary layer cannot be much deeper than their maximum depths of origin (~250 km). These observations suggest that the chemical boundary layer beneath cratons extends to ~175 km, and that the thermal boundary layer (which includes the chemical boundary layer) extends to greater depths, but not significantly exceeding ~250 km. These depth constraints are consistent with the results of more recent seismic studies. Gung et al. showed that there is pronounced radial seismic anisotropy beneath continents in the depth range of 250–400 km, which they attribute to the presence of a low viscosity asthenospheric channel [44]. Niu et al. showed that there are no detectable deflections at the 410- and 670-km discontinuities beneath the Kaapvaal craton in south Africa, which they argue limit the thickness of the Kaapvaal craton to less than ~300 km [45]. The consistent results from independent techniques provide some affirmation that our interpretations may be robust.

3. Dynamic effects of a preexisting chemical boundary layer beneath continents

We now address the dynamic effects of a compositionally and rheologically stratified thermal boundary layer beneath cratons. Fig. 2B shows the density structure of the cratonic mantle as a function of depth relative to the fertile convecting mantle (Mg#=0.89) and time since the initiation of boundary layer cooling (Fig. 2A). The density–Mg# scalings of Lee [25] were used. Cratons are assumed to be underlain by a uniformly depleted (Mg#=0.925) chemical boundary layer, which has a lower intrinsic density than the fertile convecting mantle; gray line in Fig. 2B). The thickness of the chemical boundary layer, δ_{CBL}, is inferred from the transition from depleted to fertile peridotites shown in Fig. 2A (170 km). Superimposed on Fig. 2A are hypothetical transient half-space conductive cooling curves. These are shown only to illustrate that the xenolith-defined geotherm matches an apparent 250 Ma transient geotherm, which is much younger than the cratons themselves. The high Mg#s characteristic of the cratonic chemical boundary layer imply such high degrees of melting that the chemically depleted boundary layer would be expected to be initially completely dehydrated (metasomatic reintroduction of H_2O is discussed below). Fig. 2C shows the viscosity structure of the mantle as a function of depth and time after the onset of conductive cooling. The viscosities of the chemical boundary layer and the underlying fertile mantle were calculated using the viscosity laws of Hirth and Kohlstedt [14] for wet and dry olivine and assuming complete dehydration of a fertile mantle at depths above the intersection between the adiabat and the dry peridotite solidus (Fig. 4).

The discontinuity in composition at δ_{CBL}~175 km is accompanied by discontinuities in intrinsic density and viscosity. Two features are apparent from Fig. 2B and C. First, because the deepest part of the thermal

boundary layer (>170 km) is fertile, this sublayer is intrinsically denser than the overlying material in the chemical boundary layer. This fertile sublayer becomes negatively buoyant once the transient conductive boundary layers in Fig. 2A pass through the base of the chemical boundary layer. The melt-depleted upper layer, on the other hand, will be positively or neutrally buoyant and provide a resisting force to convective downwelling. Second, the hydrated character of fertile mantle renders it over 2 orders of magnitude less viscous [14] than the chemically depleted and dehydrated mantle lying directly above it (Fig. 2C). According to Lenardic and Moresi [46] and Sleep [18], the combination of chemical buoyancy and enhanced viscosity in the chemical boundary layer is sufficient to keep the chemical boundary layer from being entrained into convective downwellings. However, the fertile and wetter sublayer is likely to be available for convection. For these reasons, we suggest that the chemical boundary layer itself is viscous (due to dehydration) and buoyant enough to act as a strong conductive lid over long timescales while the underlying fertile part represents the actively convecting part of the thermal boundary layer, which we term here the convective sublayer. The thermal boundary layer therefore consists of a strong upper lid (chemical boundary layer) and the convectively active lower portion (e.g., the convective sublayer; Fig. 3), i.e., $\delta_{TBL}=\delta_{CBL}+\delta_{CSL}$.

The thickness of the convective sublayer δ_{CSL} is linked to the thermal state of the cratonic thermal boundary layer due to the temperature-dependency of viscosity. If we assume that cratonic chemical boundary layers are so long-lived that their thermal structures have reached statistical steady state, δ_{CSL} must depend on the convective vigor in the interior of the Earth (as represented by the bottom and internally heated Rayleigh numbers) and any sources of heat generation within the cratonic chemical boundary layer as both parameters dictate the thermal state of the chemical boundary layer. Cooper et al. [21] conducted numerical simulations to explore the thermal coupling between strong chemical boundary layers and the convecting mantle at statistically steady-state conditions. They showed that the thickness of strong, preexisting chemical boundary layers dictate the nature of the thermal boundary layer beneath cratons. Fig. 3 shows that the ratio of thermal

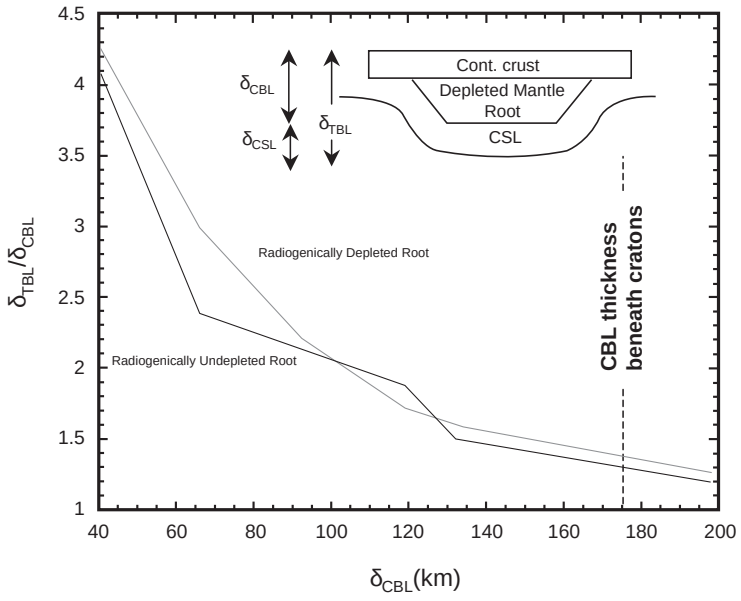

Fig. 3. The ratio of thermal boundary layer thickness to chemical boundary layer thickness for both a radiogenically undepleted (solid black line) and depleted (light gray line) cratonic root. Based on numerical simulations of Cooper et al. [21]. Inset shows schematic illustration of the relationship between the thicknesses of the chemical boundary layer (σ_{CBL}), convective sublayer (σ_{CSL}), and thermal boundary layer (σ_{TBL}). The chemical boundary layer consists of the crust and depleted mantle root, which together serve as a strong conductive lid.

boundary layer thickness to chemical boundary layer thickness $\delta_{TBL}/\delta_{CBL}$ decreases as δ_{CBL} increases. For a δ_{CBL}~175 km, such as beneath Siberia and South Africa (Fig. 2A), the numerical simulations predict a steady-state δ_{CSL} of ~50 km, which corresponds to δ_{TBL}~220 km. This is remarkably close to δ_{TBL} estimated from thermobarometric studies of mantle xenoliths (Fig. 2A), which supports the idea that the chemical boundary layer beneath a craton represents a strong, long-lived lid.

4. The chemical boundary layer beneath oceanic crust

We now address whether oceanic crust might also be underlain by a chemical boundary layer and whether this boundary layer influences the evolution of the oceanic thermal boundary layer. Unlike cratonic mantle, which can be characterized using mantle xenoliths, there are no xenolith samples of oceanic mantle. Ophiolites and abyssal peridotites provide a window to the oceanic mantle, but sample only the shallow veneer lying just beneath the Moho. We thus infer the chemical structure of oceanic mantle by assuming that it forms as the residue of partial melting beneath mid-ocean ridges, which are driven by passive upwelling (Fig. 4). Schematic streamlines of passive corner flow are shown in Fig. 4A. The intersection of the mantle adiabat and the mantle solidus represents the depth at which dry melting initiates and the peridotite residue can be said to be completely dehydrated.

Using the parameterizations of the mantle solidus taken from Hirschmann [47], it can be seen from Fig. 4 that the depth of dry melting initiates at 50 km and 110 km for solid mantle adiabats having respective potential temperatures T_P of 1300 °C and 1450 °C (T_P is defined as the temperature of the solid upper mantle if it were decompressed adiabatically to the surface), which spans the range the range of upper mantle T_P (see Section 5). The density structure of the oceanic mantle due to partial melting can also be estimated. Assuming passive upwelling and a linear melting function, the cumulative fraction of melt extracted per unit depth, dF/dz, is approximately 0.0035/km [48]. The Mg# of the mantle residue as a function of depth can be estimated by plugging $F(z)$ into an equation relating Mg# to F determined from the thermodynamically based pMELTS program (dMg#/dF ~0.0794) [49]. We can then use density–Mg# relationships [25] to infer the intrinsic density structure of the schematized oceanic mantle in Fig. 4A.

Figs. 5A–C show the density and viscosity structure of oceanic mantle for different transient geotherms (Fig. 5A). By construct of our partial melting model for mid-ocean ridges, the Mg# of the oceanic mantle decreases gradually with depth so that

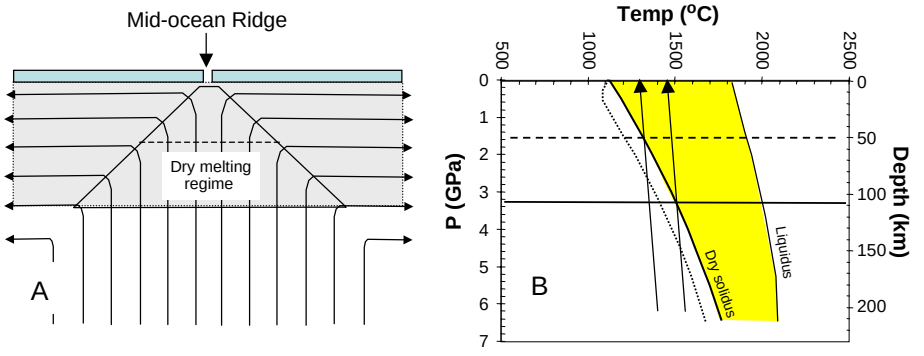

Fig. 4. (A) Schematic diagram showing how a triangular melting regime forms beneath a mid-ocean ridge undergoing passive upwelling (arrowed lines represent schematic streamlines). Due to corner flow, this results in a chemically depleted and dehydrated boundary layer. (B) Pressure–temperature diagram illustrating the geometry of adiabatic mantle ascent paths and the dry peridotite solidus. Dotted line represents the solidus for peridotite having ~700 ppm H_2O [48]. Ascent paths for two different potential temperatures (1300 and 1450 °C) are shown (adiabatic gradient of 0.5 °C/km assumed). The intersections of the adiabats and the dry solidus [47] represent the depth at which dry melting initiates. Dashed and solid horizontal lines represent the thicknesses of the resulting dehydrated and melt-depleted residuum. This leads to a strong chemical boundary layer as shown in panel (A).

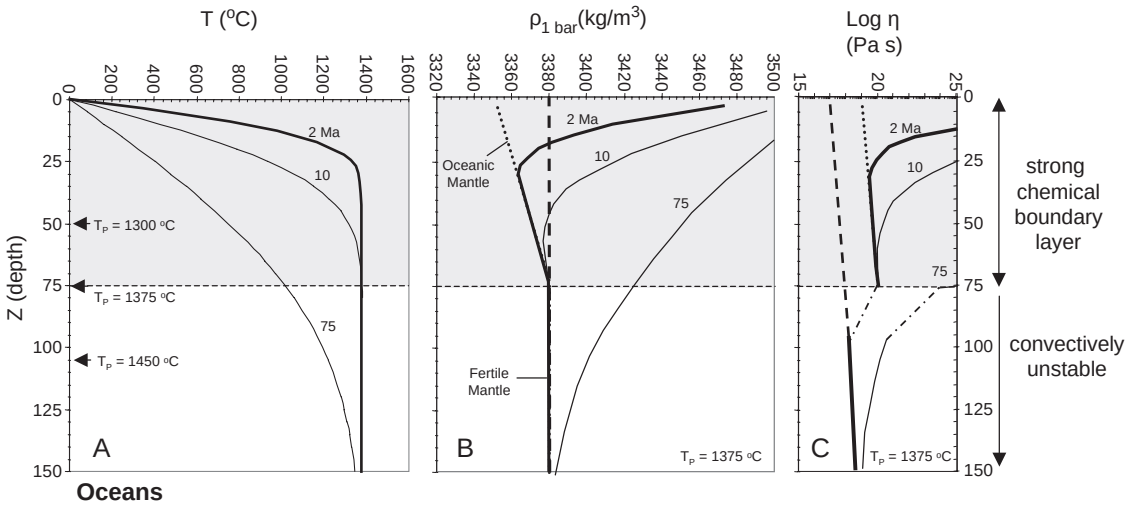

Fig. 5. (A) Transient geotherms based on a boundary layer cooling model. Horizontal dashed lines in panels (A, B, and C) show the base of a possible chemical boundary layer (shaded region) beneath which lies fertile mantle (unshaded region). (B) Pressure-normalized density structure of the mantle underlying oceans. Dotted line represents the intrinsic density structure of the oceanic mantle as estimated by the amount of partial melt extracted as a function of depth, which yields a gradational density structure (potential temperature T_P assumed to be 1375 °C). For reference, dashed line represents the density of fertile mantle at T_P and equivalent depths. Solid curves represent the density structures of oceanic mantle and underlying fertile mantle for different transient geotherms. (C) Log viscosity structure of the oceanic mantle for different transient thermal states (viscosity laws as in Fig. 2). Dash-dotted lines represent the transition from wet mantle (~700 ppm H_2O) to dry mantle. Dotted line represents the viscosity of dehydrated oceanic mantle at T_P. Dashed line shows the reference viscosity if the oceanic mantle was considered fertile.

the density structure is also gradational. Unlike cratonic mantle (Fig. 2B), there is no discontinuity in Mg# or intrinsic density in the mantle underlying oceanic crust. As a consequence, the entire oceanic mantle becomes negatively buoyant within 20 Ma (e.g., subductable) because the thermal effects outweigh the chemical effects (Fig. 5B). There is, however, a steep transition in viscosity at the base of the chemical boundary layer (Fig. 5C) as first pointed out by Hirth and Kohlstedt [14]. Depending on how hot the ambient mantle is (e.g., T_P), the thickness of this dehydrated layer can range between ~50 and 110 km (Fig. 4).

We speculate that the high viscosity and slight chemical buoyancy of the oceanic chemical boundary layer makes it unavailable for secondary convection and hence it effectively behaves as a vertically conductive lid [46]. Korenaga and Jordan [4] have investigated the more general case of depth varying intrinsic viscosity and chemical buoyancy. We examine the endmember in which the chemical boundary layer is assumed from the outset to be perfectly conducting such that it is never available for secondary convection. This assumption further implies that the thickness of the conductive layer is constant, simply reflecting the depth at which the mantle adiabat originally crossed the solidus. Of interest here is how the thickness of this conductive layer influences the onset of convective instability as the thermal boundary layer grows. Without doing any calculations, our basic assumption (e.g., constant thickness of conductive lid) yields the obvious prediction that the base of thermally defined boundary layer must eventually cross-over the base of the chemical boundary layer as the former cools. It follows that the onset time of convective instability can only postdate the time it takes for the thermally defined boundary layer to cool through the chemical boundary layer. This is because the effect of a predefined strong lid is to suppress the onset time of convective instability.

The thermal state beneath oceans, unlike the cratonic case, cannot be predicted by assuming the coupling between oceans and the convective interior

of the Earth has reached statistical steady state. Because of the short timescales involved (<200 Ma), we assume that the development of local convective instabilities at the base of the growing oceanic thermal boundary layer is largely independent of the length scale of convection in the Earth's whole mantle. We assume that the onset of convective instability can be estimated by considering a local boundary layer Rayleigh number (*Ra*). We further assume that all of the thermal boundary layer lying deeper than the base of the strong chemical boundary layer is potentially available for secondary convection, but none of the chemical boundary layer is available. If these assumptions hold, then the length scale of interest is the thickness of the entire sublayer, which we define as the convective sublayer δ_{CSL}. We note that for strongly temperature-dependent viscosity, not all of the sublayer can participate in secondary convection. This is because if the chemical boundary layer is very thin (or nonexistent), then the upper part of the convectively active sublayer would be too cold and hence too viscous to participate in secondary convection. Our model is thus only valid for the case in which all of the sublayer participates in convection.

Within the range in which our assumptions are approximately valid, we define the following scaling for the local boundary layer *Ra*:

$$Ra(t,\delta_{CBL}) \approx \frac{\rho_o \alpha g \Delta T_{CSL}(t,\delta_{CBL})[\delta_{CSL}(t,\delta_{CBL})]^3}{\kappa \mu(t,\delta_{CBL})} \quad (1)$$

where ρ_o is the intrinsic density of the convective sublayer (3380 kg/m^3), α is thermal expansivity (3×10^{-5} °C^{-1}), g is gravitational acceleration, κ is thermal diffusivity (10^{-6} m^2/s), ΔT_{CSL} is the temperature difference across the convective sublayer, μ is the "average" viscosity of the convective sublayer dictated by the average temperature of the convective sublayer, δ_{CBL} is the thickness of the preexisting chemical boundary layer, and t is the time since instantaneous cooling of the surface (Fig. 6A). For an isoviscous system and no preexisting strong chemical boundary layer, Eq. (1) simplifies to the conventional boundary layer Rayleigh number. When a preexisting chemical boundary layer of thickness δ_{CBL} exists (Fig. 6), ΔT_{CSL}, δ_{CSL}, and μ must depend on t_c and δ_{CBL} as follows. Assuming that the temperature profile of the oceanic thermal boundary layer is due

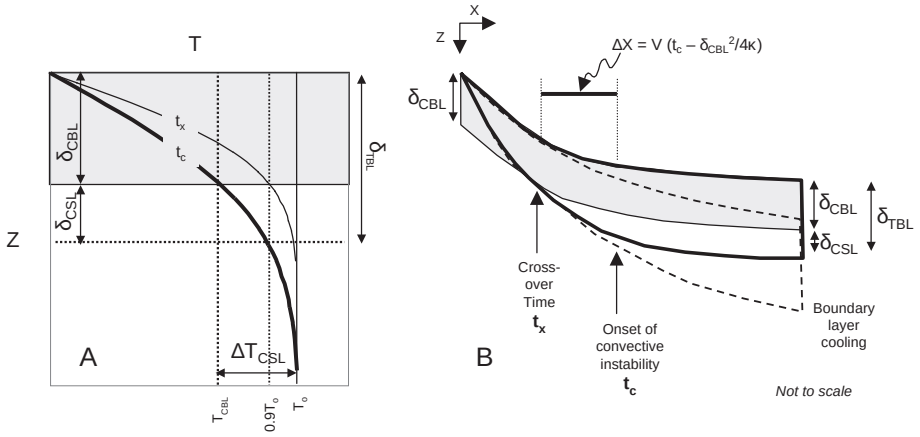

Fig. 6. A. Schematic diagram illustrating how δ_{CBL}, δ_{CSL}, and δ_{TBL} are defined just before the onset of convective instability (*T*—temperature, *Z*—depth). Solid curved line is calculated by boundary layer conductive cooling of an infinite half-space. Gray region represents the strong chemical boundary layer. (B) Schematic and exaggerated cartoon of the thermal and compositional structure beneath the seafloor (only half of the seafloor is shown). Gray region represents the high viscosity, depleted oceanic chemical boundary layer, which has a fixed thickness. Dashed region represents the growth of the thermal boundary layer as predicted by the boundary layer cooling model. Region bounded by the solid black line represents the observed thermal boundary layer thickness. The crossover time t_x predates the onset of convective instability t_c. The distance between the crossover point and the onset of convection is given by Δx, which is a function of the plate velocity v.

solely to boundary layer cooling up until t_c, the temperature difference across the convective sublayer can then be defined as the difference between the temperature at the base of the chemical boundary layer (T_{CBL}) and the temperature of the convecting interior of the mantle (T_o):

$$\frac{\Delta T_{CSL}(t_c,\delta_{CBL})}{T_o} = \frac{T_o - T_{CBL}(t_c,\delta_{CBL})}{T_o} = \mathrm{erfc}\left(\frac{\delta_{CBL}}{\sqrt{4\kappa t_c}}\right) \quad (2)$$

Defining the base of the thermal boundary layer δ_{TBL} as the depth at which the temperature equals 0.9 T_o, we can express the thickness of the convective sublayer as

$$\delta_{CSL}(t_c,\delta_{CBL}) = \delta_{TBL}(t_c) - \delta_{CBL} = 2.32\sqrt{\kappa t_c} - \delta_{CBL} \quad (3)$$

Assuming Newtonian viscosity, the average viscosity of the convective sublayer is taken as

$$\mu(t_c,\delta_{CBL}) = \mu_o \exp\left[\frac{E}{R}\left(\frac{1}{T_{CSL}^{ave}(t_c,\delta_{CBL})} - \frac{1}{T_o}\right)\right] \quad (4)$$

where μ_o is the viscosity (Pa s) at T_o, E is the activation energy (kJ/mol), R is the gas constant, and T_{CSL}^{ave} is the average temperature across the convective sublayer ($T_{CSL}^{ave} \sim T_o - 0.5\Delta T_{CSL}$).

Convective instability initiates when Ra approaches Ra_c, the critical Rayleigh number, e.g.,

$$Ra_c(t_c,\delta_{CBL}) \approx \frac{\rho_o \alpha g \Delta T_{CSL}(t_c,\delta_{CBL})[\delta_{CSL}(t_c,\delta_{CBL})]^3}{\kappa\mu(t_c,\delta_{CBL})} \quad (5)$$

where t_c represents the onset time of convective instability. Substituting Eqs. (2) (3) (4) into Eq. (1), it can be seen that the onset time of convection t_c must depend on the thickness of the chemical boundary layer, δ_{CBL}. For a given δ_{CBL}, Eq. (5) can be solved for t_c by assuming an appropriate value of Ra_c. Since we do not know the exact value of Ra_c, an approximate value of 1500 was assumed. As expected, Fig. 7A shows that t_c increases as δ_{CBL} increases since the preexisting lid suppresses the onset of convective instability.

We note that Eq. (5) (or 1) breaks down as δ_{CBL} approaches zero (Fig. 7A). Under these conditions and

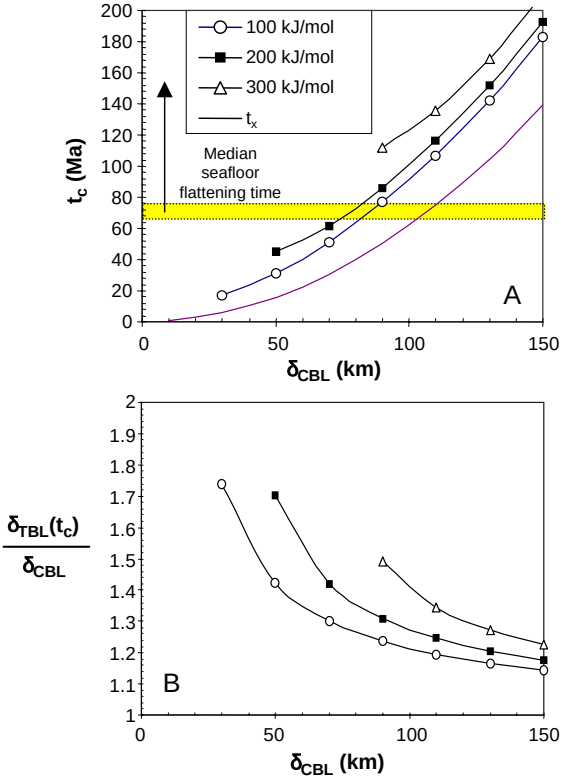

Fig. 7. (A) The critical time t_c (Ma) for the onset of convective instability as a function of chemical boundary layer thickness δ_{CBL} (km) determined by solving Eq. (1) for Ra_c=1500. Curves denoted with symbols represent Newtonian temperature-dependent viscosities assuming a μ_0 of 10^{18} Pa s and activation energies E of 100, 200 and 300 kJ/mol. The μ_0 of 10^{18} Pa s is consistent with the viscosity of the convecting mantle shown in Figs. 2C and 5C. Horizontal bar represents the median onset time for seafloor flattening; arrow shows total range of observed onset times for seafloor flattening. (B) The ratio of the thermal boundary layer and chemical boundary layer thickness at the onset of convective instability as a function of chemical boundary layer thickness. Symbols as in panel (A).

for a temperature-dependent viscosity, not all of the sublayer is available for secondary convection because the upper part of the sublayer is cold and hence highly viscous. Because our definition of T_{CSL}^{ave} assumes that all of the sublayer is available for convective instability, the average temperature of the true convective part of the sublayer is underestimated and viscosity overestimated when the thickness of the chemical boundary layer approaches zero. Thus, when δ_{CBL} approaches zero, we generate an artifact of unusually high onset times of convective instability as

can be seen from the breakdown of the curves in Fig. 7A. The artifact is most pronounced for highly temperature-dependent viscosities (e.g., high activation energy), and, as can be seen from Fig. 7A, the breakdown of our curves depend accordingly on E. However, for the conditions (thick δ_{CBL}) in which our scalings are approximately valid, it can be seen that the dependency of t_c on activation energy E is small. The low dependency on E in this endmember scenario follows from the fact that for thick chemical boundary layers, the average sublayer temperature is high and the temperature variation within the sublayer (and hence viscosity variation) is small. The small dependency with E is similar to the results of recent numerical simulations [4,5,20].

We recognize that scaling analyses by construct cannot provide absolute predictions. Nevertheless, scaling analyses can provide qualitative and relative predictions. The significance of our model is that it makes simple predictions on the relative magnitudes of potentially observable parameters, such as the thickness of the chemical boundary layer (δ_{CBL}), thickness of the thermal boundary layer (δ_{TBL}), and onset time of convective instability (t_c). First, the base of the thermally defined boundary layer should cross the base of the chemical boundary layer at a time equivalent to the time it takes for the conductive geotherm to cool just past the base of the chemical boundary layer (e.g., t_x in Fig. 6B); the distance of the cross-over point from the mid-ocean ridge should be correlated with plate velocity. Second, the onset time of convective instability, t_c, should depend on δ_{CBL} as shown in Fig. 7A. Third, the ratio of the thicknesses of the thermal boundary layer to the chemical boundary layer $\delta_{TBL}(t_c)/\delta_{CBL}$ at the onset time of convective instability should correlate with δ_{CBL} (Fig. 7B). Finally, the thickness of the oceanic chemical boundary layer, δ_{CBL}, should increase as a function of potential temperature T_P at the time the chemical boundary layer formed (see Fig. 4), which can be estimated from major-element geochemistry and/or olivine thermometry of primary mid-ocean ridge basalts (cf. [50]). This means that all of the above quantities (δ_{CBL}, δ_{TBL}, and t_c) should also correlate with T_P. Assuming that the rheologic properties of the actively convecting part of the upper mantle are globally similar (since the dependency on activation energy is small, this is not a bad assumption), our model further predicts that a plot of $\delta_{TBL}(t_c)/\delta_{CBL}$ versus onset time of convective instability throughout the seafloor should yield a negative correlation as shown in Fig. 7B. What our model cannot predict is the absolute seafloor bathymetry because our model does not explicitly account for changes in the thermal state of the underlying asthenosphere as a consequence of secondary convection [51].

Recently, Korenaga and Jordan [52] argued that the presence of a rheologically strong dehydrated boundary layer should not have any effect on the onset time of convective instabilities because it is much thinner (50–60 km) than the thickness of the rigid (highly viscous) layer at the onset time of convective instability predicted by their numerical models (~80–120 km for E=300 kJ/mol). We note, however, that the thickness of their assumed chemical boundary layer (50–60 km) was calculated for a single mantle potential temperature of 1350 °C. A higher mantle potential temperature, e.g., 1400–1450 °C, would predict chemical boundary layer thicknesses up to ~100 km. Indeed, the temperatures of the mantle source regions to mid-ocean ridge basalts have been argued previously to vary by ~250 °C [50]. In Section 5, we show that potential temperatures beneath mid-ocean ridges can be as high as ~1450 °C.

5. Testing the predictions

5.1. Continents

The predictions we make for continents and oceans can be tested only if δ_{CBL} and δ_{TBL} can be measured. For continents, we have shown above that these quantities can be estimated from thermobarometric studies of mantle xenoliths (Fig. 2) and that model predictions of Cooper et al., assuming the chemical boundary layer is intrinsically strong [21], are consistent with the observations from xenoliths. Another approach is to use seismology. A recent study on the compositional dependencies of peridotite seismic velocities at standard temperature and pressure conditions (STP) suggests that the ratio of compressional to shear wave velocity (V_P/V_S) is sensitive to Mg# but not so sensitive to temperature, provided anelastic effects are small and there is no partial melt [25]. This is because of the opposite signs of $d\ln(V_P/V_S)/dT$ for

orthopyroxene and olivine, the dominant minerals in melt-depleted peridotites. If these STP composition–velocity relationships hold at elevated pressure and temperature, one can use V_P/V_S variations to infer compositional structure. In contrast, because V_P and V_S alone are more sensitive to temperature than composition, it may be possible to use V_P, V_S, and or surface wave seismology to infer the thermal structure. In a recent study of V_P/V_S ratios using S-P travel time residuals in the South African craton, we have shown that the regional differences in V_P/V_S may in fact be correlated with differences in mantle fertility [45].

5.2. Oceans

For oceanic mantle, the degree of depletion is less than that seen in cratonic mantle, and the compositional and mineralogic transition at the base of the chemical boundary layer is much more gradational than beneath cratons. For these reasons, it will be difficult to seismically separate the base of the chemical and thermal boundary layers beneath the oceans.

Another way to estimate δ_{CBL} beneath oceans is from the intersection depth of the mantle adiabat with the dry peridotite solidus. The depth of intersection can be calculated from the mantle's paleo-potential temperature (e.g., the temperature at the surface of the Earth if the laterally averaged upper mantle were isentropically decompressed) and solid adiabat. Constraints on the potential temperature can be estimated from the compositions of primary magmas [50,53,54]. One caveat is that the liquidus temperatures of mid-ocean ridge basalts are undoubtedly minimum estimates of mantle potential temperature because they have cooled along nonadiabatic paths, as evidenced by the fact they have already undergone significant crystallization of olivine (and in some cases, clinopyroxene and plagioclase) by the time they are sampled. The temperature of magma segregation from the mantle can only be had by estimating primary magma compositions after correcting for differentiation effects. This is done by incrementally adding equilibrium olivines back into a magma (e.g., reversing fractional crystallization) with the constraint that $K_D=(Fe/Mg)^{ol}/(Fe/Mg)^{melt}=0.31$. The assumption is that olivine is the only crystallizing phase. For mid-ocean ridge basalts having MgO contents greater than 8 wt.% MgO, this is generally a reasonable assumption because crystallization takes place at low pressure where the olivine liquidus surface is greatly expanded. When the Mg# of the magma reaches equilibrium with an olivine having typical upper mantle compositions (in this case, Mg# of 0.89–0.90 was assumed), it is assumed that the primary magma composition has been attained. The MgO and SiO_2 content of this primary magma is then used to respectively calculate the average temperature [55] and pressure [56] of the magma when it was last equilibrated with the mantle. For temperature, this means that both FeO and MgO are important parameters. For those mid-ocean ridge basalts having high FeO for a given MgO content (hence low Mg#s), larger amounts of olivine must be added to reach equilibrium with typical upper mantle olivines (Mg#=0.89–0.90), giving rise to primary magma compositions having higher MgO contents and accordingly, higher magmatic temperatures due to the proportionality of magmatic temperature with MgO [55].

The potential temperature is then calculated in two steps. First, the P-T path of the primary magma is back-tracked to the solidus along an isentropic decompressional melting path (under reversible conditions, this is equivalent to an adiabatic melting path). The approach requires simultaneous numerical integration of $(dX/dP)_S$ and $(dT/dP)_S$, which represent the differentials of melt fraction X and T as a function of P at constant entropy (S) using the formulas presented in McKenzie [57] and the updated solidus and liquidus P-T relations in Hirschmann [47] and Katz et al. [58]. The intersection of the melting adiabat with the dry peridotite solidus is then used as an anchor point for the solid mantle adiabat, and the potential temperature of the solid mantle is then calculated by integrating $(dT/dP)_S$ following McKenzie and Bickle [54].

As a preliminary test of our oceanic hypothesis, we have examined the compositions of old oceanic crust (>50 Ma) in the western Pacific Ocean (Pacific plate only) and the western half of the northern Atlantic (North American plate only; north of equator; Fig. 8A). According to Marty and Cazenave [10], seafloor depth begins to deviate from the half-space cooling model between 70 and 100 Ma in the western Pacific and between 100 and 150 Ma in the northern Atlantic. In Fig. 8B–D, we have plotted FeO and MgO contents

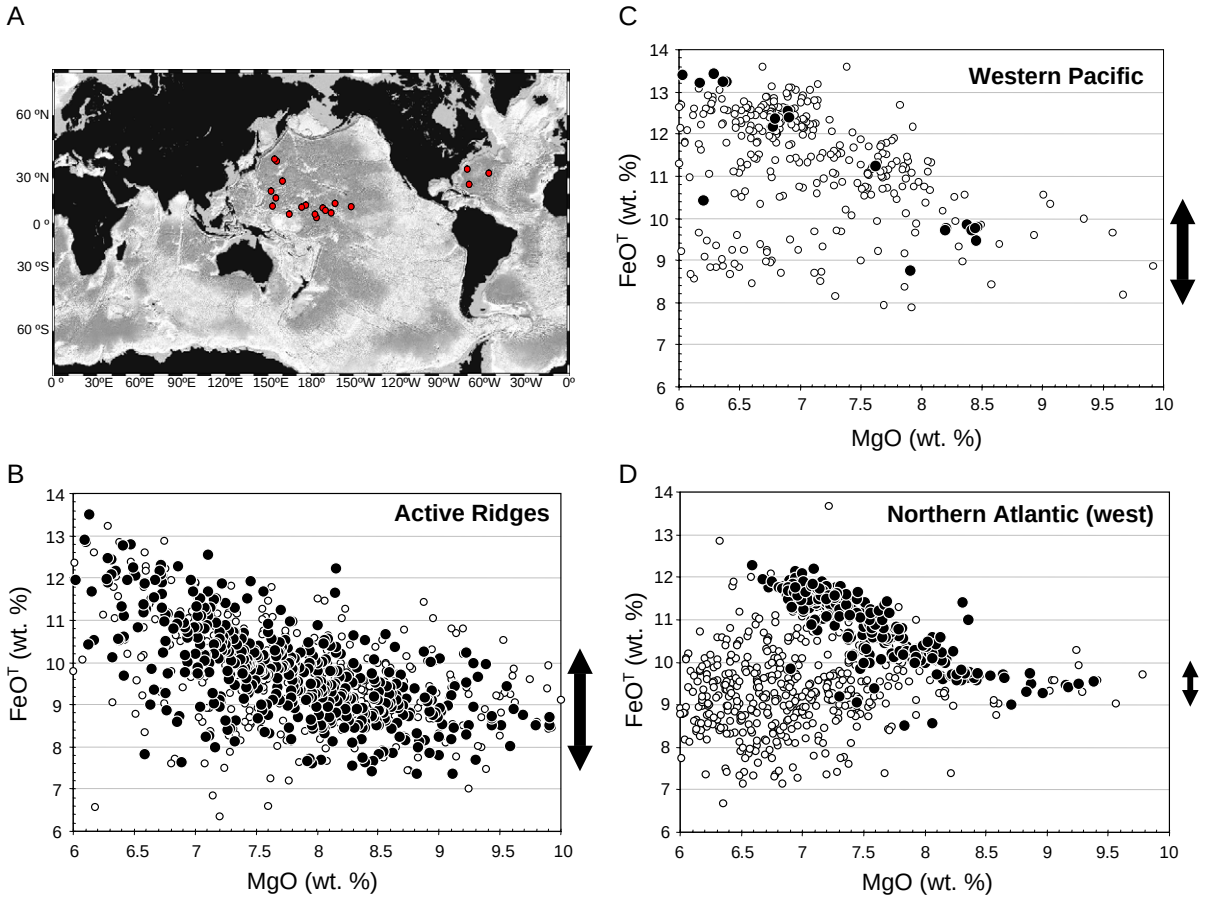

Fig. 8. (A) Sample localities. (B) FeO and MgO contents of whole-rock (open symbols) and glass (solid symbols) mid-ocean ridge basalt samples from active ridges (Juan de Fuca, East Pacific Rise, mid-Atlantic, Indian; [59]). Vertical bars (with arrowed ends) show estimated range of FeO at MgO>8.5 wt.%. (C) and (D) FeO and MgO contents of old oceanic crust (>50 Ma) in the western Pacific and western half of the northern Atlantic (e.g., north of the equator) using data from [59]. Symbols as in panel (B).

from active ridges and old oceanic crust (>50 Ma) in the two regions of interest using the data from RidgePetDB [59]. Both fresh glass and whole-rock data are represented. Fresh glass is considered superior to whole-rock data because the latter have been chemically modified by seawater alteration. The effects of seawater alteration are most pronounced for old oceanic crust.

For MgO>8 wt.%, the FeO contents of basaltic glasses from active ridges (mid-Atlantic, East Pacific Rise, Juan de Fuca, and Southeast Indian) range between 7.5 and 10 wt.% (Fig. 8B). There are no new data for glasses having MgO>8 wt.% in the western Pacific (Fig. 8C). However, if we take the few western Pacific whole-rock data points at face value, it appears that their FeO contents overlap the range of active ridges. In contrast, for old oceanic crust in the northern Atlantic, the glasses have FeO contents ranging between 9 and 10 wt.% (Fig. 8D), which falls in the upper end of the compositional range seen in active ridges (and old Pacific crust). The average segregation pressures and temperatures of the primary magma compositions inferred from the basaltic data are shown in Fig. 9A along with their corresponding mantle potential temperatures (Fig. 9A and B). It can be seen that active ridges and old Pacific crust yield potential temperatures between 1330 and 1450 °C, whereas old oceanic crust in the northern Atlantic crust yields paleo-potential temperatures of 1410–1450 °C.

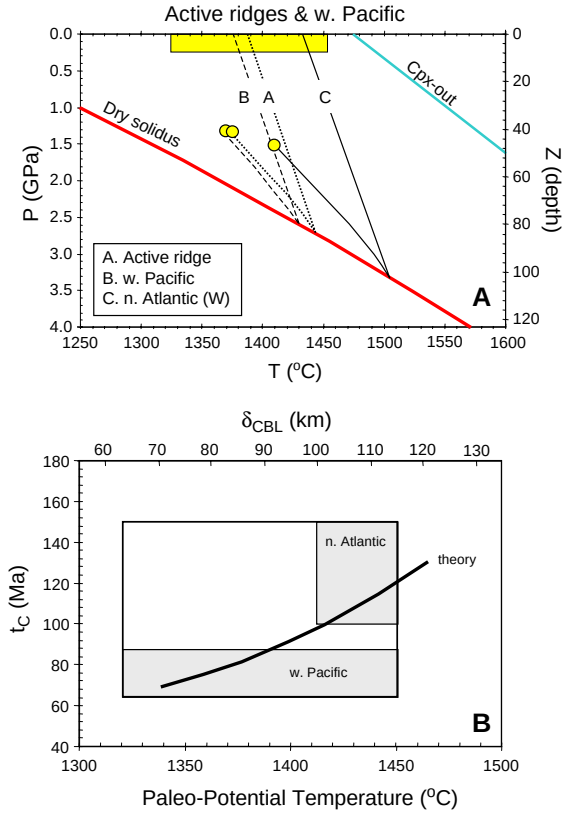

Fig. 9. (A) Pressure (GPa) versus temperature (°C) diagram showing the estimated mantle segregation temperatures and pressures (●) of the primary parental magmas to the basaltic compositions shown in Fig. 8B–D. Lines connecting each solid circle to the dry peridotite solidus [58] represent anhydrous melting adiabats; lines connecting the intersection of the melting adiabat with the dry solidus to the surface represent solid mantle adiabats; the temperature at the surface of the Earth is the potential temperature. Horizontal shaded bar represents the range of potential temperatures seen in modern mid-ocean ridge basalts. Line labeled Cpx-out represents the point at which clinopyroxene is completely exhausted from the residue [58]. (B) Plot of the range of paleo-potential temperatures (°C) estimated for old oceanic crust in the western Pacific and western half of the northern Atlantic (shaded boxes) versus the range of onset times t_c for seafloor flattening in the respective regions [10]. Large open box encompassing the shaded boxes for the western Pacific and western half of the northern Atlantic represents the global range of t_c and modern mantle potential temperature. Top horizontal axis represents the equivalent thickness of the dehydrated chemical boundary layer. Curves represent relative dependency of onset time for convective instability versus thickness of the preexisting chemical boundary layer from Fig. 7.

In Fig. 9B, we plot the potential temperatures (with estimated uncertainties) of active ridges, old oceanic crust in the western Pacific and western part of the northern Atlantic versus the total range in onset times of observed seafloor flattening in the respective regions. On the top axis of Fig. 9B, the corresponding chemical boundary layer thickness is plotted. The large range in potential temperature for old Pacific crust is due to the large scatter in the data. However, it can be seen that the northern Atlantic falls in the upper right hand corner of the total range of seafloor flattening times and modern potential temperature. If the onset time of seafloor flattening represents the onset time of convective instability, then the high mantle potential temperatures and long onset times for seafloor flattening are consistent with the predictions of our scaling arguments. This can be seen from Fig. 9B, where we have superimposed our theoretical prediction. We reemphasize that the absolute position of this curve is meaningless, but the relative sense of the curve is meaningful.

We readily admit that these preliminary observations are not extremely convincing. Clearly, more fresh glass data from old oceanic crust are needed. We also recognize that another uncertainty in our interpretation of old oceanic crust data rests on the assumption that the mantle source composition to mid-ocean ridge basalts is constant. If it is not, then an alternative explanation is that the FeO contents of the mantle sources to old Pacific and Atlantic oceanic crust are different, rendering our estimates of paleo-potential temperature meaningless. This means that, in addition to more major-element data on fresh glasses, complementary trace-element and isotopic data are needed to track variations in source heterogeneity. If these data can become available in the near future, geochemical constraints on chemical boundary layer thicknesses can be combined with seismic constraints on the thickness of oceanic thermal boundary layers (e.g., surface wave seismology [60]). This would allow for an estimate of the ratio $\delta_{TBL}(t_c)/\delta_{CBL}$ for a given region of oceanic lithosphere, providing yet another approach for testing our model.

6. Conclusions and implications

Our analyses suggest that chemical boundary layers play a significant role in dictating the thickness of thermal boundary layers beneath oceans and continents. For continents, the thermal boundary layer

thickness at statistical steady state is limited by the thickness of a preexisting chemical boundary layer, which represents a highly melt-depleted, dehydrated mantle layer. For oceans, a new model is presented that relates the transition between a vertically conductive heat transfer regime and a convection-dominated regime to the thickness of a preexisting chemical boundary layer. The chemical boundary layer beneath oceans originates by melt extraction at mid-ocean ridges, which yields a melt-depleted (but not as depleted as most cratonic mantle) and dehydrated mantle layer that is consequently strong from the outset like that beneath continents. The thickness of the oceanic chemical boundary layer is a function of potential temperature and therefore, the proposed model makes specific predictions on the relationships between the onset of seafloor flattening and various geochemical indices that indirectly track potential temperature (e.g., FeO and MgO).

If our models are correct, the thermal and structural evolution of continents and oceans must be controlled in part by the presence of preexisting chemical boundary layers. This implies further that chemical boundary layers may indirectly dictate the strength of continental and oceanic thermal boundary layers because the integrated strength of any thermal boundary layer depends on its intrinsic viscosity (hypothesized here to be primarily controlled by water content) and average temperature, which itself depends on its thickness (as well as the distribution of radiogenic heat production). Thick, dehydrated and melt-depleted chemical boundary layers would be expected to give rise to strong lithosphere, while thin, wetter, and more fertile chemical boundary layers would be expected to give rise to weaker lithosphere [68]. It thus follows that there may be a relationship between the degree of intraplate deformation (e.g., diffuse plate deformation) and the thickness and composition of preexisting chemical boundary layers.

One important point that we did not discuss was how chemical boundary layers actually form beneath continents. While the formation of a dehydrated layer beneath mid-ocean ridges can be explained by a relatively simple model, how cratonic mantle formed is still open to debate. On one hand, the thicker and more depleted nature of the chemical boundary layer beneath cratons might imply formation by melting of upwelling mantle characterized by significantly higher temperatures than the present (e.g., [13,61,62]). This process allows for the generation of a thick and dehydrated chemical boundary layer in one relatively short geologic event. However, it has been suggested that cratonic peridotites may have actually melted at pressures significantly less (<3 GPa) than their present equilibration pressures (>3 GPa) as they do not show the tell-tale trace-element signatures of garnet [63,64]. In addition, it is not clear if mantle potential temperature was significantly hotter in the late Archean [65], and finally, the presence of dipping seismic reflectors within cratonic mantle are highly suggestive of trapped oceanic lithosphere [66]. These observations can be reconciled if cratonic mantle is formed by amalgamation or thickening of oceanic lithosphere (as well as arc lithosphere). However, if these lithospheric segments are initially dry, a paradox arises because they should be strong and not easily deformed. If they are wet or rehydrated to make them weak enough to deform and make cratons, another paradox arises because a chemically buoyant boundary layer, without being intrinsically stronger, would eventually thin out gravitationally (e.g., in the spirit of [67]).

Acknowledgments

This work was supported by the Department of Earth Science at Rice University and NSF grants to Lee (EAR-0309121) and Lenardic (EAR-0001029). J. Dixon and J. Korenaga are thanked for their reviews. Informal discussions with J. Korenaga, S. Zhong, and W. Leeman are greatly appreciated.

References

[1] J.G. Sclater, B. Parsons, Oceans and continents: similarities and differences in the mechanisms of heat loss, J. Geophys. Res. 86 (1981) 11535–11552.
[2] B. Parsons, D.P. McKenzie, Mantle convection and the thermal structure of the plates, J. Geophys. Res. 83 (1978) 4485–4495.
[3] W.H.F. Smith, D.T. Sandwell, Global sea floor topography from satellite altimetry and ship depth soundings, Science 277 (1997) 1956–1962.
[4] J. Korenaga, T.H. Jordan. Onset of convection with temperature- and depth-dependent viscosity, Geophys. Res. Lett. 29, (2002).

[5] J. Huang, S.J. Zhong, J. van Hunen, Controls on sub-lithospheric small-scale convection, Journ. Geophys. Res. (2003).
[6] C.A. Stein, S. Stein, A model for the global variation in oceanic depth and heat flow with lithospheric age, Nature 359 (1992) 123–129.
[7] C.A. Stein, S. Stein, Comparison of plate and asthenospheric flow models for the thermal evolution of oceanic lithosphere, Geophys. Res. Lett. 21 (1994) 709–712.
[8] J. Phipps Morgan, W.H.F. Smith, Flattening of the seafloor depth-age curve as a response to asthenospheric flow, Nature 359 (1992) 524–527.
[9] G.F. Davies, Dynamic Earth, Plates, Plumes and Mantle Convection, Cambridge University Press, Cambridge, UK, 1999, 458 pp.
[10] J.C. Marty, A. Cazenave, Regional variations in subsidence rate of oceanic plates: a global analysis, Earth Planet. Sci. Lett. 94 (1989) 301–315.
[11] R.T. Heest, S.T. Crough, The effect of hot spots on the oceanic age-depth relation, J. Geophys. Res. 86 (1981) 6107–6114.
[12] T.H. Jordan, Composition and development of the continental tectosphere, Nature 274 (1978) 544–548.
[13] H.N. Pollack, Cratonization and thermal evolution of the mantle, Earth Planet. Sci. Lett. 80 (1986) 175–182.
[14] G. Hirth, D.L. Kohlstedt, Water in the oceanic upper mantle; implications for rheology, melt extraction and the evolution of the lithosphere, Earth Planet. Sci. Lett. 144 (1–2) (1996) 93–108.
[15] R.J. Walker, R.W. Carlson, S.B. Shirey, F.R. Boyd, Os, Sr, Nd, and Pb isotope systematics of southern African peridotite xenoliths: implications for the chemical evolution of subcontinental mantle, Geochim. Cosmochim. 53 (1989) 1583–1595.
[16] D.G. Pearson, R.W. Carlson, S.B. Shirey, F.R. Boyd, P.H. Nixon, Stabilisation of Archaean lithospheric mantle: a Re–Os isotope study of peridotite xenoliths from the Kaapvaal craton, Earth Planet. Sci. Lett. 134 (1995) 341–357.
[17] S.E. Zaranek, E.M. Parmentier, Convective cooling of an initially stably stratified fluid with temperature-dependent viscosity: implications for the role of solid-state convection in planetary evolution, J. Geophys. Res. 109 (2004).
[18] N.H. Sleep, Survival of Archean cratonal lithosphere, J. Geophys. Res. 108 (2003).
[19] A. Davaille, C. Jaupart, Onset of thermal convection in fluids with temperature-dependent viscosity: application to the oceanic mantle, J. Geophys. Res. 99 (1994) 19853–19866.
[20] J. Korenaga, T.H. Jordan, Physics of multiscale convection in Earth's mantle: onset of sublithospheric convection, J. Geophys. Res. 108 (B7) (2003) 2333.
[21] C.M. Cooper, A. Lenardic, L. Moresi, The thermal structure of stable continental lithosphere within a dynamic mantle, Earth Planet. Sci. Lett. 222 (2004) 807–817.
[22] F.R. Boyd, Compositional distinction between oceanic and cratonic lithosphere, Earth Planet. Sci. Lett. 96 (1989) 15–26.
[23] W.L. Griffin, S.Y. O'Reilly, C.G. Ryan, The composition and origin of sub-continental lithospheric mantle, Mantle Petrology: Field Observations and High Pressure Experimentation: A Tribute to R. (Joe) Boyd 6, Geochemical Society, 1999, pp. 13–45.
[24] F.R. Boyd, R.H. McAllister, Densities of fertile and sterile garnet peridotites, Geophys. Res. Lett. 3 (1976) 509–512.
[25] C.-T.A. Lee, Compositional variation of density and seismic velocities in natural peridotites at STP conditions: implications for seismic imaging of compositional heterogeneities in the upper mantle, J. Geophys. Res. 108 (2003) 2441.
[26] T.H. Jordan, Structure and formation of the continental tectosphere, J. Petrol. 1988 (1988) 11–37.
[27] S.Y. O'Reilly, W.L. Griffin, Y.H. Djomani, P. Morgan, Are lithospheres forever? Tracking changes in subcontinental lithospheric mantle through time, GSA Today 11 (4) (2001) 4–10.
[28] F.R. Boyd, N.P. Pokhilenko, D.G. Pearson, S.A. Mertzman, N.V. Sobolev, L.W. Finger, Composition of the Siberian cratonic mantle: evidence from Udachnaya peridotite xenoliths, Contrib. Mineral. Petrol. 128 (1997) 228–246.
[29] M.G. Kopylova, J.K. Russell, H. Cookenboo, Petrology of peridotite and pyroxenite xenoliths from Jericho Kimberlite; implications for the thermal state of the mantle beneath the Slave Craton, northern Canada, J. Petrol. 40 (1) (1999) 79–104.
[30] D.R. Bell, Water in mantle minerals, Nature 357 (1992) 646–647.
[31] D.R. Bell, G.R. Rossman, Water in Earth's mantle: the role of nominally anhydrous minerals, Science 255 (1992) 1391–1397.
[32] J.E. Dixon, L. Leist, C. Langmuir, J.-G. Schilling, Recycled dehydrated lithosphere observed in plume-influenced mid-ocean-ridge basalt, Nature 420 (2002) 385–389.
[33] J.E. Dixon, T.H. Dixon, D.R. Bell, R. Malservisi, Lateral variation in upper mantle viscosity: role of water, Earth Planet. Sci. Lett. 222 (2004) 451–467.
[34] S.P. Grand, R. van der Hilst, S. Widiyantoro, Global seismic tomography; a snapshot of convection in the Earth, GSA Today 7 (1997) 1–7.
[35] D.E. James, M.J. Fouch, J.C. VanDecar, S. van der Lee, Tectospheric structure beneath Southern Africa, Geophys. Res. Lett. 28 (2001) 2485–2488.
[36] S.B. Shirey, J.W. Harris, S.R. Richardson, M.J. Fouch, D.E. James, P. Cartigny, P. Deines, F. Viljoen, Diamond genesis, seismic structure, and evolution of the Kaapvaal–Zimbabwe craton, Science 297 (2002) 1683–1686.
[37] J. Polet, D.L. Anderson, Depth extent of cratons as inferred from tomographic studies, Geology 23 (1995) 205–208.
[38] C.J. Wolfe, I.T. Bjarnason, J.C. Van Decar, S.C. Solomon, Assessing the depth resolution of tomographic models of upper mantle structure beneath Iceland, Geophys. Res. Lett. 29 (2002).
[39] W.R. Keller, D.L. Anderson, R.W. Clayton, Resolution of tomographic models of the mantle beneath Iceland, Geophys. Res. Lett. 27 (2000) 3993–3996.
[40] R.L. Rudnick, W.F. McDonough, R.J. O'Connell, Thermal structure, thickness and composition of continental lithosphere, Chem. Geol. 145 (1998) 395–411.
[41] C.-T. Lee, R.L. Rudnick, Compositionally stratified cratonic lithosphere: petrology and geochemistry of peridotite xenoliths from the Labait tuff cone, Tanzania, in: B.J. Dawson volume,

J.J. Gurney, J.L. Gurney, M.D. Pascoe, S.R. Richardson (Eds.), Proc. VIIth International Kimberlite Conference, 1999, pp. 503–521.

[42] F.R. Boyd, High- and low-temperature garnet peridotite xenoliths and their possible relation to the lithosphere-asthenosphere boundary beneath southern Africa, in: P.H. Nixon (Ed.), Mantle Xenoliths, John Wiley and Sons, 1987, pp. 403–412.

[43] M.J. Walter, Melting residues of fertile peridotite and the origin of cratonic lithosphere, in: Y. Fei, C.M. Bertka, B.O. Mysen (Eds.), Mantle Petrology: Field Observations and High Pressure Experimentation: A Tribute to Francis R. (Joe) Boyd, Geochemical Society Special Publication, vol. 6, 1999, pp. 225–239.

[44] Y. Gung, M. Panning, B. Romanowicz, Global anisotropy and the thickness of continents, Nature 422 (2003) 707–711.

[45] F. Niu, A. Levander, C.M. Cooper, C.-T.A. Lee, A. Lenardic, D.E. James, Seismic constraints on the depth and composition of the mantle keel beneath the Kaapvaal craton, Earth Planet. Sci. Lett. 224 (2004) 337–346.

[46] A. Lenardic, L.N. Moresi, Some thoughts on the stability of cratonic lithosphere; effects of buoyancy and viscosity, J. Geophys. Res. B, Solid Earth Planets 104 (6) (1999) 12,747–12,759.

[47] M.M. Hirschmann, Mantle solidus: experimental constraints and the effects of peridotite composition, Geochem. Geophys. Geosys. 1 (2000) (2000GC000070).

[48] P.D. Asimow, C.H. Langmuir, The importance of water to oceanic mantle melting regimes, Nature 421 (2003) 815–820.

[49] M.S. Ghiorso, M.M. Hirschmann, P.W. Reiners, V.C. Kress, The pMELTS: a revision of MELTS for improved calculation of phase relations and major element partitioning related to partial melting of the mantle to 3 GPa, Geochem. Geophys. Geosys. 3 (2002).

[50] E.M. Klein, C.H. Langmuir, Global correlations of ocean ridge basalt chemistry with axial depth and crustal thickness, J. Geophys. Res. 92 (B8) (1987) 8089–8115.

[51] R.J. O'Connell, B.H. Hager, On the thermal state of the earth, in: A. Dziewonski, E. Boschi (Eds.), Physics of the Earth's interior, 1980, pp. 270–317.

[52] J. Korenaga, T.H. Jordan, On 'steady-state' heat flow and the rheology of oceanic mantle, Geophys. Res. Lett., 29 (2002).

[53] E. Humler, C. Langmuir, V. Daux, Depth versus age: new perspectives from the chemical compositions of ancient crust, Earth Planet. Sci. Lett. 173 (1999) 7–23.

[54] D. McKenzie, M.J. Bickle, The volume and composition of melt generated by extension of the lithosphere, J. Petrol. 29 (1988) 625–679.

[55] T. Sugawara, Empirical relationships between temperature, pressure, and MgO content in olivine and pyroxene saturated liquid, J. Geophys. Res. 105 (2000) 8457–8472.

[56] F. Albarède, How deep do common basaltic magmas form and differentiate? J. Geophys. Res. 97 (1992) 10997–11009.

[57] D. McKenzie, The generation and compaction of partially molten rock, J. Petrol. 25 (3) (1984) 713–765.

[58] R.F. Katz, M. Spiegelman, C.H. Langmuir, A new parameterization of hydrous mantle melting, Geochem. Geophys. Geosys., 4 (2003).

[59] K. Lehnert, Y. Su, C.H. Langmuir, B. Sarbas, U. Nohl, A global geochemical database structure for rocks, Geochem. Geophys. Geosys. 1 (2000) (1999GC000026).

[60] M.H. Ritzwoller, N.M. Shapiro, S.-J. Zhong, Cooling history of the Pacific lithosphere, Earth Planet. Sci. Lett. 226 (2004) 69–84.

[61] M.J. Walter, Melting of garnet peridotite and the origin of komatiite and depleted lithosphere, J. Petrol. 39 (1998) 29–60.

[62] C. Herzberg, Phase equilibrium constraints on the formation of cratonic mantle, in: Y. Fei, C.M. Bertka, B.O. Mysen (Eds.), Mantle Petrology, Field Observations and High Pressure Experimentation, A Tribute to Francis R. (Joe) Boyd, Geochem. Soc. Spec. Pub., vol. 6, 1999, pp. 241–257.

[63] D. Canil, Mildly incompatible elements in peridotites and the origins of mantle lithosphere, Lithos 77 (2004) 375–393.

[64] S. Bernstein, P.B. Kelemen, C.K. Brooks, Depleted spinel harzburgite xenoliths in Tertiary dykes from East Greenland: restites from high degree melting, Earth Planet. Sci. Lett. 154 (1998) 221–235.

[65] T.L. Grove, S.W. Parman, Thermal evolution of the Earth as recorded by komatiites, Earth Planet. Sci. Lett. 219 (2004) 173–187.

[66] M. Bostock, Mantle stratigraphy and evolution of the Slave province, J. Geophys. Res. 103 (1998) 21183–21200.

[67] P. Bird, Lateral extrusion of lower crust from under high topography, in the isostatic limit, J. Geophys. Res. 96 (1991) 10275–10286.

[68] C.-T. Lee, Q. Yin, R.L. Rudnick, S.B. Jacobsen, Preservation of ancient and fertile lithospheric mantle beneath the southwestern United States, Nature 411 (2001) 69–73.